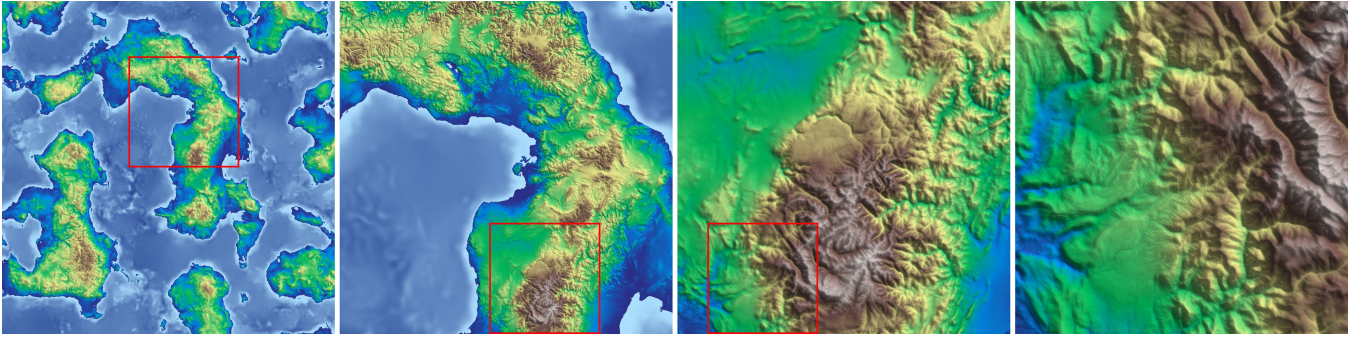


# Terrain Diffusion: A Diffusion-Based Successor to Perlin Noise in Infinite, Real-Time Terrain Generation

Alexander Goslin

alexander.goslin@gmail.com

Website: <https://xandergos.github.io/terrain-diffusion>



**Figure 1:** A region of a world generated with Terrain Diffusion. The leftmost panel spans roughly five million square kilometers, with about 2.2 million square kilometers of land area, comparable to the size of the Congo. Red boxes denote the region shown in the next panel, illustrating coherent terrain generation across four orders of magnitude in scale. Zoom for details.

## Abstract

For decades, procedural worlds have been built on procedural noise functions such as Perlin noise, which are fast and infinite, yet fundamentally limited in realism and large-scale coherence. We introduce Terrain Diffusion, a generative framework that bridges the fidelity of diffusion models with the properties that made procedural noise indispensable: seamless infinite extent, seed-consistency, and constant-time random access. At its core is InfiniteDiffusion, a novel algorithm for infinite generation that reformulates standard diffusion sampling for unbounded domains. While noise functions remain near-instant, our framework outpaces orbital velocity by 9× on a consumer GPU, enabling realistic terrain generation at interactive rates. We integrate a hierarchical stack of diffusion models to couple planetary context with local detail, a compact Laplacian encoding to stabilize outputs across Earth-scale dynamic ranges, and an open-source infinite-tensor framework for constant-memory manipulation of unbounded tensors. Together, these components position diffusion models as a practical, scalable foundation for the next generation of infinite virtual worlds.

## 1 Introduction

Procedural terrain generation underpins the creation of virtual worlds, from open-world games to planetary simulations. For nearly four decades, procedural noise functions such as Perlin noise [23, 24] have defined this field. They offer three properties that make them indispensable for procedural worlds: seamless infinite extensibility, seed-consistency, and constant-time random access. A single random seed can deterministically produce a boundless landscape without storing vast datasets, providing an elegant foundation for procedural worlds.

Yet these procedural methods are inherently limited. Their patterns are smooth and lack the hierarchical organization of real

geography. Continents, mountain ranges, and river basins emerge in nature from structured, multi-scale processes that simple noise cannot capture. As a result, worlds built from procedural noise often appear plausible but not real.

Recent advances in generative modeling, particularly diffusion models [12, 27], have transformed image synthesis by learning to reproduce natural structure with remarkable realism and control, but these methods are typically confined to smaller bounded domains. Recent work has explored infinite or large-scale generation capabilities, but these approaches generally lose one or more of the core properties that make procedural noise valuable in interactive applications.

Terrain Diffusion addresses these limitations through InfiniteDiffusion, a generalization of MultiDiffusion [2] for infinite inference. Our framework retains the functional utility of noise while leveraging diffusion models for realism far beyond the reach of procedural noise.

A hierarchical diffusion stack unifies global and local structure: a coarse planetary model establishes continental structure, refined by higher-resolution models that introduce mountain ranges, valleys, and local relief. A novel elevation encoding further stabilizes training and inference across the full dynamic range of Earth’s terrain. Few-step consistency distillation [21, 28] enables rapid inference, and an open-source infinite-tensor framework enables constant-memory streaming and composable manipulation of infinite tensors.

Together, these components establish the first learned system capable of streaming an entire planet in real time on consumer GPUs. Terrain Diffusion demonstrates that diffusion models can serve as a practical foundation for infinite, seed-consistent worlds that can be explored interactively and without restrictions.

**Table 1: Capability Matrix. Comparison of InfiniteDiffusion against procedural and generative baselines.**

Method	Infinite	Deterministic	Speed	Quality
Procedural Noise	✓	✓	Instant	Low
InfinityGAN [20]	✓	✓	Fast	Limited*
Standard Diffusion	✗	✓	Slow	High
Auto-Regression	✓	✗	$O(n)$	High
<b>Ours</b>	✓	✓	<b>Fast</b>	<b>High</b>

\*Prone to training instability and mode collapse.

## 2 Related Works

**Procedural noise.** Procedural terrain traditionally relies on procedural noise such as Perlin or Simplex noise [23, 24], often combined with fractal Brownian motion (fBm) [8]. These methods remain popular for their controllability, speed, seed-consistency, and infinite extent, but they lack the large-scale structure of real landscapes. They produce repetitive, texture-like patterns and cannot reproduce complex features such as mountain ranges, branching valleys, or volcanic and glacial landforms without extensive post-processing.

**Diffusion and consistency models.** Denoising diffusion models [12, 27] generate samples by iteratively refining noise and are widely used for high-fidelity synthesis. Consistency models [28] approximate denoised diffusion outputs in one or a few steps, and continuous variants [21] achieve throughput competitive with GANs while retaining most of the quality of full diffusion sampling, enabling interactive use cases.

**Learned terrain generation.** GAN-based terrain models [1, 3, 9, 29, 30] can generate convincing local relief, but they operate on fixed crops and do not tile, limiting them to bounded worlds. Diffusion-based synthesis [5, 10, 13] further improves fidelity and control, but also assumes finite canvases and requires relatively significant compute. Jain et al. [14] offers infinite terrain generation by sampling diffusion-based tiles and blending them with a Perlin-based kernel. Because tiles are generated independently and the kernel has no awareness of broader context, structure remains tied to perlin noise rather than the learned model. In contrast, Terrain Diffusion couples all tiles through a shared global context and fuses tiles through a fully learned, context-aware mechanism. Procedural noise is used only for defining continental layouts, where data is sparse and simple enough that more complex alternatives would provide little benefit while reducing user control.

**MultiDiffusion and unbounded generation.** Several works extend generative models beyond image bounds seen in training. InfinityGAN [20] produces infinite images with GANs but does not extend to diffusion models, limiting scalability. MultiDiffusion [2] and Mixture of Diffusers [15] generate images larger than the training canvas but still assume a bounded final extent. Auto-regressive methods such as BlockFusion [31] and WorldGrow [19] generate worlds by conditioning each tile on its neighbors, producing continuous worlds but without seed consistency, since outputs depend on sampling order. Additionally, tiles must be produced sequentially, preventing efficient random access. In contrast, we define

a seed-consistent InfiniteDiffusion algorithm whose outputs are order invariant and allow constant-time random-access generation over an infinite domain.

## 3 InfiniteDiffusion: Unbounded Generation Across Planetary Scales

MultiDiffusion [2] provides a simple and effective way to extend diffusion sampling beyond a model’s native resolution by averaging predictions from overlapping windows. This enables synthesis across larger images, as local predictions fuse into a seamless image. However, in its standard form, MultiDiffusion remains confined to bounded domains: all windows must lie within a fixed finite canvas, limiting its applicability to unbounded worlds or continuously streamed environments.

We introduce InfiniteDiffusion, an extension of MultiDiffusion that lifts this constraint. By reformulating the sampling process to operate over an effectively infinite domain, InfiniteDiffusion supports seamless, consistent generation at scale. The remainder of this section reviews the principles of MultiDiffusion, and formalizes its extension to unbounded domains. We present the definitions in  $\mathbb{Z}^2$  for clarity, but all results extend to  $\mathbb{Z}^d$  with minimal modification.

### 3.1 A Review of MultiDiffusion

MultiDiffusion extends standard diffusion sampling by averaging overlapping windows, producing consistent outputs from local predictions. Each denoising step aggregates the predictions of overlapping patches, enforcing continuity across window boundaries and allowing generation of regions much larger than a model’s input size. The process begins with a pretrained diffusion model  $\Phi$ , operating on images in  $\mathcal{I} = \mathbb{R}^{H \times W \times C}$ . The diffusion process generates a sequence of images

$$I_T, I_{T-1}, \dots, I_0 \quad \text{s.t.} \quad I_{t-1} = \Phi(I_t | y)$$

that refines the original noisy image  $I_T$  into a fully denoised version  $I_0$ , under conditioning vector  $y$ . MultiDiffusion defines a new model  $\Psi$  that generates in a different image space  $\mathcal{J} = \mathbb{R}^{H' \times W' \times C}$ , producing a new sequence of images

$$J_T, J_{T-1}, \dots, J_0 \quad \text{s.t.} \quad J_{t-1} = \Psi(J_t | z).$$

To accomplish this, MultiDiffusion defines  $n$  windows indexed by  $i \in [n]$ . In the finite setting, a region  $R$  is any rectangular subset of the  $H' \times W'$  coordinate grid, while a window region has a fixed size  $H \times W$ . In MultiDiffusion, each window  $i$  is assigned a window region  $R_i$ . For an image  $J \in \mathcal{J}$ , we write  $J[R]$  for the values of  $J$  on the coordinates in  $R$ .

Each window also has a weight matrix  $W_i \in \mathbb{R}^{H \times W}$  that specifies the relative contribution of each pixel in the pretrained diffusion model’s output. Let  $U_i(x)$  denote the  $H' \times W'$  image that places an  $H \times W$  tensor  $x$  in the region  $R_i$  with zeros elsewhere. With these definitions, the closed form MultiDiffusion update for direct pixel or latent-space samples is

$$\Psi(J_t | z) = \frac{\sum_{i=1}^n U_i(W_i \otimes \Phi(J_t[R_i] | y_i))}{\sum_{j=1}^n U_j(W_j)} \quad (1)$$

where  $\otimes$  denotes the Hadamard product. This expression represents a weighted average of all local denoising predictions, where each window contributes according to its weight map. The result is a

global update that reconciles all overlapping diffusion paths into a single image.

Although MultiDiffusion elegantly unifies local diffusion paths, it remains constrained to bounded domains: the process assumes a finite number of windows and requires the pretrained diffusion model to be evaluated at all windows to complete one step. Extending the same principle to infinite domains therefore requires reformulating  $\Psi$  so that it operates locally and independently of global window layouts, a key step towards the InfiniteDiffusion algorithm introduced next.

### 3.2 From MultiDiffusion to InfiniteDiffusion

We now seek to extend MultiDiffusion beyond finite image domains. We first redefine the MultiDiffusion image space as an unbounded image,  $\mathcal{J} = \mathbb{R}^{\mathbb{Z} \times \mathbb{Z} \times C}$ , so that generation produces an infinite output. Consequently, we now define a region to be any rectangular subset of  $\mathbb{Z}^2$ . Since generation is now over an infinite domain, window indices must now range over a countably infinite set  $S$ .

For all applications shown in this work, we take  $S = \mathbb{Z}^2$ , so each window is indexed by  $(i, j)$ , and each window region  $R_{ij}$  is defined as a square sliding window with side length  $H = W$  and stride  $s$  on both axes. Concretely,  $R_{ij} = [is, is + H) \times [js, js + W)$ . This particular layout is not essential to the InfiniteDiffusion formulation and serves only as an implementation choice for the experiments.

With an infinite number of windows, the MultiDiffusion update becomes intractable, and computation requires an infinite sum to produce the final image. Instead, we seek to generate the image lazily, by only evaluating particular regions  $R$ .

To achieve this, we define  $\kappa$  to be the function mapping a region to the set of window indices that overlap it. We assume  $|\kappa(R)|$  is always finite. This enables the InfiniteDiffusion update

$$\Psi(J_t | z)[R] = \left( \frac{\sum_{i \in \kappa(R)} U_i(W_i \otimes \Phi(J_t[R_i] | y_i))}{\sum_{j \in \kappa(R)} U_j(W_j)} \right) [R], \quad (2)$$

which is the MultiDiffusion update with only the windows intersecting  $R$  evaluated. In the finite setting, the full image  $J_t$  can be generated in advance, making each  $J_t[R_i]$  effectively free. In the infinite setting, precomputing  $J_t$  is impossible, so evaluating  $J_t[R_i]$  requires recursively invoking the same update. A naive implementation would therefore incur exponentially growing compute. To avoid this, we cache intermediate window computations across queries.

### 3.3 Practical Querying of InfiniteDiffusion

To make queries practical, we avoid recomputing the same window updates across recursive calls. Instead, for each image  $J_t$  we maintain two corresponding infinite tensors:  $A_t$ , which stores the numerator in Eq. 2, and  $B_t$ , which stores the denominator. Both tensors are initialized to zero. These infinite tensors are typically stored in tiles, which can be loaded and unloaded as necessary to conserve memory. When a query  $J_t[R]$  occurs, we identify all the windows required to generate the region, and process all previously unprocessed windows, populating the desired regions of  $A_t$  and  $B_t$ . Then  $J_t[R] = A_t[R]/B_t[R]$ . Final generation proceeds as a recursive process that begins by sampling  $J_T$  as Gaussian noise.  $J_0[R]$  is obtained by recursively applying the query routine at all

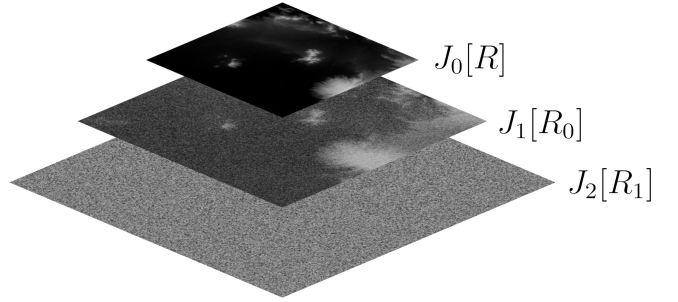


**Figure 2: A conceptual visualization of InfiniteDiffusion with sliding windows. The user’s query  $J_0[R]$  induces a deterministic chain of window queries: computing  $J_0[R]$  requires a region  $J_1[R_0]$ , which in turn requires a region  $J_2[R_1]$ . Querying  $J_2[R_1]$  is inexpensive since it corresponds directly to Gaussian noise.**

earlier steps. In summary, Algorithm 1 below computes  $J_t[R]$  by evaluating only the windows that overlap  $R$ , caching each window’s contribution in  $A_t$  and  $B_t$ , so that future queries can reuse the same results. The tensors  $A_t$ ,  $B_t$ , and the set of processed windows  $P_t$  are mutated in-place. See Figure 2 for a visualization.

---

**Algorithm 1** Querying  $J_t[R]$  ( $t < T$ ) with InfiniteDiffusion.

---

**Inputs:**

- $\Phi$      $\triangleright$  pretrained diffusion model
- $J_{t+1}$   $\triangleright$  infinite noisy input image
- $A_t$      $\triangleright$  infinite accumulated output image
- $B_t$      $\triangleright$  infinite accumulated weights for  $A_t$
- $R$       $\triangleright$  region to query
- $P_t$      $\triangleright$  set of processed windows

**for** each window  $i$  in  $\kappa(R) \setminus P$  **do**

- $A_t[R_i] \leftarrow A_t[R_i] + W_i \otimes \Phi(J_{t+1}[R_i] | y_i)$
- $B_t[R_i] \leftarrow B_t[R_i] + W_i$

**end for**

$P_t \leftarrow P_t \cup \kappa(R)$

**Output:**  $J_t[R] = A_t[R]/B_t[R]$

---

### 3.4 Tractability via Truncated $T$

There is one final but critical barrier in making InfiniteDiffusion practical. Each query  $J_t[R]$  typically requires a region of  $J_{t+1}$  larger than  $R$  itself, as pixels near the edge of  $R$  are generated by windows that extend beyond  $R$ . In the sliding-window case, regions grow quadratically in area, yielding an overall  $O(T^3)$  time complexity for final generation. For traditional MultiDiffusion, which relies on continuously fusing diffusion paths over dozens of steps, this complexity renders infinite generation effectively impossible.

To overcome this, we redefine  $\Phi$  as an arbitrary denoising function, such as a few-step Consistency Model or a sequence of standard diffusion steps, rather than a single atomic step. This insight decouples  $T$  from the internal diffusion schedule, which may be much longer.

Crucially, we find that our framework retains striking coherence even when generation is aggressively truncated to  $T = 1$  or  $2$ . We hypothesize that because global structure is largely determined from hierarchical conditioning, overlapping windows only need to enforce local consistency that is already largely aligned through shared noise. Additionally, our models are trained on random crops, so they learn an approximately translation invariant representation that bases predictions on local patterns, which are shared across overlapping windows, rather than absolute position, further reducing seams. Together, these factors make the method robust even under minimal iterative refinement.

### 3.5 Properties of InfiniteDiffusion

*Formal proofs for all properties are provided in Appendix B*

*Seed consistency.* A central property of InfiniteDiffusion is that it preserves the seed-consistent behavior that makes procedural noise functions useful for procedural world generation. Seed consistency follows directly from how the process is defined. Once a seed is fixed, the initial noise image  $J_T$  is completely determined. The query routine is a deterministic function of its inputs, so  $J_t$  is a deterministic function of  $J_{t+1}$ , and caching only memoizes intermediate results of this deterministic computation. This argument requires that the conditioning variables  $y_i$  are themselves seed-consistent, which is typically trivial when  $y_i$  is constant or generated by the same InfiniteDiffusion algorithm, as in this work. By composing these steps, every image  $J_t$  and every region  $J_t[R]$  becomes a fixed function of the original seed. In particular, requesting the same region again, or in a different order relative to other regions, always returns exactly the same value, since the computation depends only on the seed and the region, not on the sequence of queries.

*Constant-time random access.* Assuming that  $|\kappa(R_i)| \leq M$  for any window region  $R_i$ , InfiniteDiffusion guarantees constant-time random access. In particular, for any window region  $R_i$ , the query  $J_0[R_i]$  is  $O(1)$ . In practice, this allows discontinuous exploration of the world: any region can be queried independently, and seed consistency ensures that skipping intermediate tiles never alters the generated content or its quality.

*Parallelization.* InfiniteDiffusion also admits parallel evaluation of window updates. For any fixed timestep  $t$ , each evaluation of  $\Phi$  is independent, so they can be batched and executed in parallel.

### 3.6 An Open Source Infinite Tensor Framework for Unbounded Inference

To support unbounded generation without exceeding memory limits, we introduce the Infinite Tensor framework<sup>1</sup>, a Python library that enables sliding window computation over tensors with infinite dimensions. It allows querying of arbitrarily large images as if they were standard PyTorch tensors while keeping only the visible region in memory. Each operation is performed through a fixed-sized sliding window that dynamically loads, evicts, or deletes data as sampling progresses. While Algorithm 1 theoretically requires unbounded storage, our framework can optionally cache operations  $\mathcal{T}[R_i] \leftarrow \mathcal{T}[R_i] + x$  directly, so  $\mathcal{T}$  is stored implicitly as a series

<sup>1</sup>Available at <https://github.com/xandergos/infinite-tensor>

of summations. Consequently, each contribution  $x$  for any window need not be persistently stored; it can be deleted and simply recomputed on demand, permitting bounded disk use.

This abstraction lets diffusion and consistency models operate directly on infinite images without manual data management. Windows can overlap to provide context and blend results, and multiple infinite tensors can depend on one another to form hierarchical pipelines. The framework serves as the runtime layer that links local model inference with practical, global world synthesis.

Together, InfiniteDiffusion and the Infinite Tensor framework provide the foundation required for practical, unbounded generation. The remaining components of Terrain Diffusion build on this foundation by combining these capabilities with large-scale real-world training data, hierarchical modeling, and a task-specific architecture.

## 4 Data

To enable truly global generation, we construct a seamless global elevation dataset merging land topography from the 90m MERIT DEM [32] and ocean bathymetry from ETOPO1 [22], supplemented by climatic data from WorldClim [7]. We process this data into equal-area tiles by dynamically stretching longitude based on latitude; this ensures that pixel sizes represent a consistent physical area, allowing the diffusion model to learn features with minimal polar distortion. The dataset is split into 2048×2048 training tiles, with specific details on coastline smoothing, bathymetric merging, and sampling heuristics provided in Appendix E.

## 5 Hierarchical Modeling & Stabilization

This section outlines the hierarchical architecture and data representation underlying our pipeline, which together enable coherent, high-fidelity terrain generation across planetary scales.

### 5.1 Signed Square-Root Transform

Terrain tiles vary significantly in elevation range. Under a fixed noise distribution, this leads to uneven effective SNR: low-relief regions behave as though exposed to stronger noise, while high-relief terrain is affected much less. In the raw elevation space, tiles with higher absolute elevations exhibit larger variance. To reduce this variation, we apply a signed square-root transform  $z \mapsto \text{sign}(z)\sqrt{|z|}$ . The transform compresses high-relief values and distributes variance across tiles more uniformly. Namely, the correlation between the mean and log standard deviation of tiles decreases from 0.66 to 0.31. In practice, this allows us to train with a more focused noise distribution and enhances the visibility of small features, especially coastlines. Additional details in Appendix F.

### 5.2 Stabilization Via Laplacian Encodings

Due to normalization, the large dynamic range of Earth elevations make model errors deceptively large in absolute units. Even relatively small errors of  $\sigma = 0.01$  can correspond to  $\pm 25\text{m}$  noise after denormalization. To mitigate this, we predict a Laplacian-based representation comprising a low-frequency component, obtained by downsampling and blurring the original image, and a residual/high-frequency component given by subtracting the upsampled low frequency component from the original image.

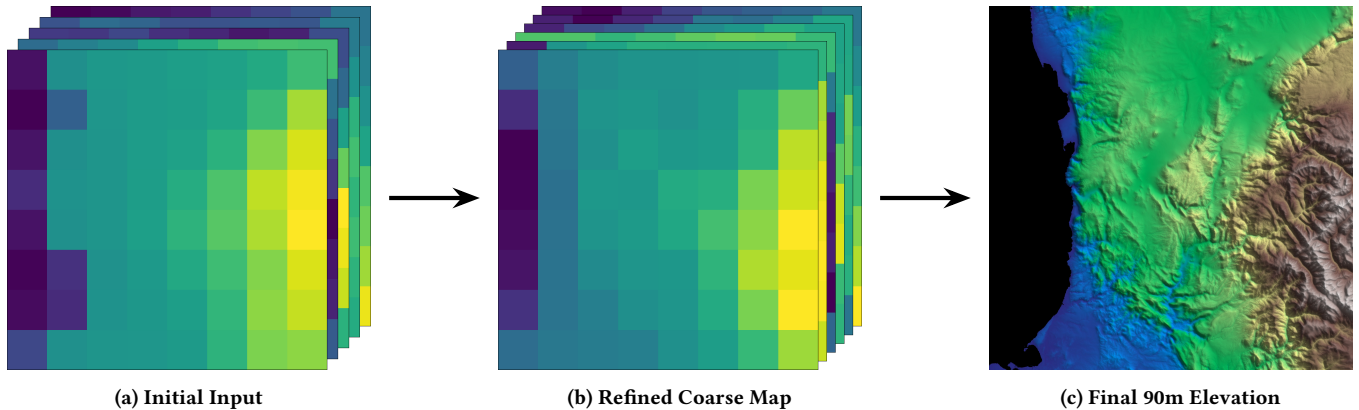


**Figure 3: Multi-stage elevation generation pipeline. (a) The initial coarse map, which serves as the structural and climatic guide. Can be made by hand or generated procedurally. (b) The refined coarse map, enhanced by our lightweight coarse model to enforce realism. (c) The final 90m elevation map generated by the core latent diffusion model, with InfiniteDiffusion for tiling.**

Residual errors are over  $30\times$  smaller in magnitude due to their lower variance. To clean the low-frequency channel after generation, we decode the noisy low- and high-frequency components ( $L + H$ ) into a provisional heightmap, then blur and downsample it to re-extract a denoised low-frequency  $\hat{L}$ , with any high-frequency noise redirected to the residual  $\hat{H}$ . Final synthesis uses  $\hat{L} + H$ , so low-frequency errors vanish while high-frequency detail is preserved. In practice,  $L \approx \hat{L}$  even under strong synthetic noise, confirming that re-extraction cleanly isolates low-frequency structure. This Laplacian denoising step reduces the FID [11] of the untiled core diffusion model (introduced next) from 21.51 to 8.11, and the corresponding consistency model, which powers our final pipeline, from 75.15 to 12.72.

### 5.3 A Hierarchical Model

Planetary terrain spans several orders of magnitude in scale, from continental structure to meter-level detail, making one-pass generation infeasible. Several previous works [6, 18, 26, 33, 34] have shown that MultiDiffusion produces repetitive results when poorly conditioned, a problem that InfiniteDiffusion inherits. We therefore organize generation into a small hierarchy of models operating at progressively finer resolutions. Each stage refines and conditions on the one above, maintaining large-scale coherence while producing realistic local detail. All models share a common EDM2 [17] backbone with the modifications proposed in sCM [21]. The hierarchy begins with a coarse planetary model, which generates the basic structure of the world from a rough, procedural or user-provided layout. The next stage is the core latent diffusion model [25], which transforms that rough structure into realistic 46km tiles in latent space. Finally, a consistency decoder expands these latents into a high-fidelity elevation map. All models are trained on random crops to learn a nearly translation-invariant representation, reflecting the fact that generation should be independent of absolute location. We visualize the coarse-to-fine pipeline in Figure 3.

The core latent diffusion model synthesizes  $512 \times 512$  patches at a 90m resolution in signed-sqrt space, corresponding to 46km tiles. It predicts a  $64 \times 64$  low-frequency elevation channel and latent map

that compactly represents the corresponding  $512 \times 512$  image. To supply the latent codes, we train a separate VAE-style autoencoder that shares the same U-Net backbone but omits diffusion-specific components and skip connections. The model is optimized using L1 and LPIPS losses with a weak KL term to prevent overfitting. After training, the encoder processes each  $2048 \times 2048$  tile in the dataset as a whole, and the resulting latent image is precomputed and stored alongside the tile. To maximize local quality, the imprecise VAE decoder is discarded, and a diffusion decoder learns to expand these latents into realistic and high-resolution residuals. Conditioning in the diffusion decoder is implemented by concatenating nearest-neighbor interpolated latents to the noisy input image at each diffusion step.

To facilitate long-range global coherence, the core model is conditioned on  $4 \times 4$  patches of elevation data. Each pixel of the patch is about 23km, with the model prediction corresponding to the  $2 \times 2$  interior. Each patch contains 3 channels: the mean elevation of the pixel, the 5th percentile elevation of the pixel, and a binary mask indicating which pixels have data available. We also provide the model with the tile’s mean temperature, temperature variation, annual precipitation, and precipitation seasonality for additional coherence and user control. Since climatic data is not available in the ocean, we replace missing values with a standard gaussian, ensuring the model accepts any combination of climatic variables in ocean regions. These values are injected into the model as a flattened vector alongside the noise embedding.

### 5.4 Real-Time Planetary Scale Synthesis

The coarse diffusion model facilitates this hierarchy by producing the conditioning variables required by the core latent model. The user provides initial maps for this model using hand-drawn sketches or procedural noise, which we found works as well as purely learned methods while providing additional control. During inference, these inputs are corrupted with gaussian noise according to the user’s preference on a per-channel basis, and concatenated against the usual diffusion inputs. The model follows the EDM2 design but with no downsampling or upsampling operations. This

limits the receptive field by design, preventing the model from drifting toward the massive continental structures present in Earth data and avoiding conflicts where global priors override user guidance while still allowing strong local corrections.

To enable real-time streaming, all diffusion models, except the coarse model, are distilled into continuous-time consistency models [21]. To improve fidelity further, we apply the guidance scheme proposed in AutoGuidance [16]. Combined, these stages form a complete generation pipeline, from planetary context to local detail, capable of on-demand, real-time synthesis.

## 6 Results

We evaluate Terrain Diffusion on visual fidelity and latency. Latency experiments use a single NVIDIA RTX 3090 Ti GPU. InfiniteDiffusion uses  $T = 2$  and a stride of 32 in the core model, and  $T = 1$  with a batch size of 1 in the coarse and decoder models. We use a separable linear weight window that is 1 at the window center and decreases linearly to a small value  $\epsilon$  at the boundary, which reduces FID from 19.32 with a constant map to 14.78. The decoder model uses windows of size 512 with strides 384. Batch size is 16 for the core model and 1 for other components.

### 6.1 Visual Fidelity

We perform internal ablations to isolate the effects of our proposed architecture. We calculate FID [11] for (1) non-tiled diffusion samples, (2) non-tiled consistency samples, and (3) tiled samples generated with InfiniteDiffusion<sup>2</sup>. This isolates base fidelity, the effect of consistency distillation, and the effect of tiling.

We also compare to Perlin blending [14], where tiles are blended with perlin noise, and naive tiling, where tiles are simply concatenated without blending. To verify the necessity of fusing diffusion paths during the generative process, we also evaluate ‘naive InfiniteDiffusion.’ In this setup, overlapping windows are generated independently as black boxes but with shared noise and conditioning, and their final outputs are linearly blended. Table 2 shows our results.

**Table 2: FID-50k for generations with InfiniteDiffusion vs. other methods. Lower is better. The distilled theoretical lower bound is underlined. The best tiled result is bolded.**

Tiling	Distilled	FID ↓
Perlin Blending [14]	✓	196.70
Naive Tiling	✓	74.44
Naive InfiniteDiffusion	✓	35.13
InfiniteDiffusion	✓	<b>14.78</b>
None	✓	<u>12.72</u>
None	×	8.11

Perlin blending yields a high FID of 196.70, confirming that standard procedural blending techniques fail to approximate the

<sup>2</sup>FID is computed on central 984×984 crops of the validation tiles to ensure adequate surrounding context. InfiniteDiffusion is applied only to the latent space; tiling the decoder would require impractically large context, and the decoder already produces near seamless outputs.

statistical distribution of natural topography. The significant fidelity gap between InfiniteDiffusion (FID 14.78) and Naive InfiniteDiffusion (FID 35.13) further demonstrates that large-scale coherence cannot be achieved by merely blending independent patches; it requires fusing intermediate paths iteratively within the latent space. Most notably, InfiniteDiffusion preserves the fidelity of the base consistency model with remarkable accuracy (14.78 vs. 12.72). This marginal FID increase indicates that our windowed fusion strategy, even with  $T=2$ , successfully maintains perceptual and spatial continuity, scaling from finite training crops to infinite worlds with little degradation in quality.

For context, we also measure the decoder’s standalone rFID at  $512 \times 512$  resolution. The one step variant obtains an rFID of 2.83, while the two step variant reaches 1.07. Tiling only increases the one-step FID to 2.99. Evaluations use raw elevation values, with images normalized by centering each tile and scaling by the larger of its value range or 255, ensuring that images are not expanded beyond the native precision of the data. All results use two-step generation for the core consistency model and one-step for the consistency decoder.

### 6.2 Latency: Time to First and Second Tile

Because generation of any fixed-size region has bounded cost, generating a contiguous  $n$ -length strip is  $O(n)$ . But neighboring tiles reuse cached context, so the cost for querying the first region is larger than for subsequent regions.

Motivated by these facts, we measure end-to-end latency as the *time to first tile* (TTFT) and *time to second tile* (TTST) across resolutions. TTFT denotes the delay from model initialization to the first tile becoming available, reflecting initial setup cost. TTST measures the time to generate an adjacent tile thereafter, reflecting interactive exploration performance. While both metrics are bounded, they vary with the specific region location because the number of intersecting windows differs across positions. To account for this, we perform 1000 runs at random locations and report the average and standard deviation.

**Table 3: Generation latency for the first and second tile.**

Region Size	TTFT	TTST
$512 \times 512$	$1.72 \pm 0.19$	$0.66 \pm 0.18$
$256 \times 256$	$1.25 \pm 0.19$	$0.26 \pm 0.18$

An F-35, one of the fastest conventional aircraft in service at roughly 550 m/s, would traverse a  $512 \times 512$  tile at 90 m resolution in about 84 seconds. In that time, Terrain Diffusion can produce 130 additional tiles. In a 1:15 miniature world, where a vehicle at highway speeds (60mph) effectively encounters terrain at 405 m/s, the system maintains a  $170 \times$  performance buffer. Even at the theoretical extreme of orbital velocity ( $\approx 7,700$  m/s), generation remains  $9 \times$  faster than traversal.

### 6.3 Qualitative Analysis

Figure 4 shows 20  $1024 \times 1024$  tiles from Terrain Diffusion, all from the same seed used for Fig. 1. The model produces sharp ridges,

visually coherent river basins, smooth transitions, and varied landscapes. No visible tiling artifacts confirm the effectiveness of InfiniteDiffusion.

To demonstrate practical use, we integrate Terrain Diffusion into the Minecraft engine by replacing the native world generator. Elevation and biome queries are routed through our model, and climatic outputs are mapped to Minecraft biomes using a light-weight rule set. The system streams terrain in real time and handles arbitrary traversal; only features that rely on long distance biome searches, such as `/locate biome` and explorer maps, remain unsupported. Runtime is dominated by Minecraft’s own generation logic rather than our model, and gameplay remains smooth even under rapid movement. Figure 5 shows representative in game terrain. For these interactive visualizations, we apply bilinear interpolation to upsample the heightmaps  $4\times$ .

## 7 Discussion

*Limitations.* The main limitation of our method arises from data scarcity at the coarsest levels of the hierarchy. Each additional level operates on a downsampled representation of the dataset, rapidly reducing the number of independent training examples available to learn large-scale structure. This can make it difficult to train a diffusion model with sufficient receptive field to enforce global coherence. This limitation is application-dependent. For natural terrain, meaningful global structure exists only at the scale of a small number of continental landmasses, making data scarcity unavoidable. In our case, externally specified procedural priors, such as Perlin noise, provide a practical source of coarse structure that is seed-consistent and controllable, while the learned hierarchy refines this signal at higher resolutions where data is abundant. In contrast, domains with effectively unbounded or tiling structure, such as textures, may support an entirely learned hierarchy.

*Comparison to procedural noise.* Although Terrain Diffusion retains the formal guarantees of procedural noise, it fundamentally diverges in fidelity and computational cost. By leveraging deep generative models, our method captures complex structural and hydrological realism that noise functions approximate only as superficial textures, with the added flexibility of retraining on new datasets to target different environments. While this comes at the cost of raw throughput compared to the microsecond-level latency of noise, our setup time of 1.72 seconds and steady-state generation time of 0.66 seconds remain highly practical. Ultimately, we do not view this as a total replacement; procedural noise retains decisive advantages in speed, interpretability, and zero-data requirements, suggesting that future systems will likely employ a hybrid approach where noise handles simple, low-latency tasks and learned models manage high-fidelity, complex structure.

## 8 Future Work

Adding features to the hierarchy is a natural next step. The coarse model, the base model, or both could incorporate additional variables such as soil properties, other climatic variables, or satellite imagery, enhancing control and enabling additional downstream applications. Resolution can also be extended by adding further refinement stages. While increased resolution does require more work for the same real-world area, traversal speed and viewing

distance often scale with resolution. In this case, the lower throughput required at low resolutions typically balances the extra work at high resolutions, making high-resolution generation highly efficient. Finally, the InfiniteDiffusion formulation itself is not specific to terrain. Any domain that can be decomposed into overlapping tiles can adopt the same sampling strategy, including textures, maps, and large environments in general.

## 9 Conclusion

We have presented Terrain Diffusion, a diffusion-based framework for coherent, real-time terrain generation across planetary scales. By reformulating MultiDiffusion for unbounded domains and introducing the Infinite Tensor framework, we enable seed-consistent, random-access synthesis of infinite worlds with constant memory and compute. A hierarchical stack of diffusion and consistency models unifies planetary organization with local realism, producing continuous landscapes far beyond the reach of procedural noise. Together, these components position diffusion models as a practical foundation for procedural worldbuilding.

## References

- [1] O. Argudo, A. Chica, and C. Andujar. 2018. Terrain Super-resolution through Aerial Imagery and Fully Convolutional Networks. *Computer Graphics Forum* 37, 2 (2018), 101–110. arXiv:https://onlinelibrary.wiley.com/doi/pdf/10.1111/cgf.13345 doi:10.1111/cgf.13345
- [2] Omer Bar-Tal, Lior Yariv, Yaron Lipman, and Tali Dekel. 2023. MultiDiffusion: Fusing Diffusion Paths for Controlled Image Generation. *arXiv preprint arXiv:2302.08113* (2023).
- [3] Christopher Beckham and Christopher Pal. 2017. A step towards procedural terrain generation with GANs. doi:10.48550/ARXIV.1707.03383 Version Number: 1.
- [4] Mikołaj Bińkowski, Dougal J. Sutherland, Michael Arbel, and Arthur Gretton. 2018. Demystifying MMD GANs. In *International Conference on Learning Representations*. <https://openreview.net/forum?id=r1IU0zWCW>
- [5] Paul Borne-Pons, Mikołaj Czerkawski, Rosalie Martin, and Romain Rouffet. 2025. MESA: Text-Driven Terrain Generation Using Latent Diffusion and Global Copernicus Data. arXiv:2504.07210 [cs.GR] <https://arxiv.org/abs/2504.07210>
- [6] Ruoyi Du, Dongliang Chang, Timothy Hospedales, Yi-Zhe Song, and Zhanyu Ma. 2024. DemoFusion: Democratizing High-Resolution Image Generation With No \$\$\$ In *CVPR*.
- [7] Stephen E. Fick and Robert J. Hijmans. 2017. WorldClim 2: new 1-km spatial resolution climate surfaces for global land areas. *International Journal of Climatology* 37, 12 (Oct. 2017), 4302–4315. doi:10.1002/joc.5086
- [8] Alain Fournier, Don Fussell, and Loren Carpenter. 1982. Computer rendering of stochastic models. *Commun. ACM* 25, 6 (June 1982), 371–384. doi:10.1145/358523.358553
- [9] Ian Goodfellow, Jean Pouget-Abadie, Mehdi Mirza, Bing Xu, David Warde-Farley, Sherjil Ozair, Aaron Courville, and Yoshua Bengio. 2020. Generative adversarial networks. *Commun. ACM* 63, 11 (Oct. 2020), 139–144. doi:10.1145/3422622
- [10] Éric Guérin, Julie Digne, Éric Galin, Adrien Peytavie, Christian Wolf, Bedrich Benes, and Benoît Martinez. 2017. Interactive example-based terrain authoring with conditional generative adversarial networks. *ACM Transactions on Graphics* 36, 6 (Dec. 2017), 1–13. doi:10.1145/3130800.3130804
- [11] Martin Heusel, Hubert Ramsauer, Thomas Unterthiner, Bernhard Nessler, and Sepp Hochreiter. 2018. GANs Trained by a Two Time-Scale Update Rule Converge to a Local Nash Equilibrium. doi:10.48550/arXiv.1706.08500 arXiv:1706.08500 [cs].
- [12] Jonathan Ho, Ajay Jain, and Pieter Abbeel. 2020. Denoising Diffusion Probabilistic Models. In *Advances in Neural Information Processing Systems*, H. Larochelle, M. Ranzato, R. Hadsell, M. F. Balcan, and H. Lin (Eds.), Vol. 33. Curran Associates, Inc., 6840–6851. [https://proceedings.neurips.cc/paper\\_files/paper/2020/file/4c5bcfec8584af0d967f1ab10179ca4b-Paper.pdf](https://proceedings.neurips.cc/paper_files/paper/2020/file/4c5bcfec8584af0d967f1ab10179ca4b-Paper.pdf)
- [13] Zexin Hu, Kun Hu, Clinton Mo, Lei Pan, and Zhiyong Wang. 2024. Terrain diffusion network: climatic-aware terrain generation with geological sketch guidance. In *Proceedings of the Thirty-Eighth AAAI Conference on Artificial Intelligence and Thirty-Sixth Conference on Innovative Applications of Artificial Intelligence and Fourteenth Symposium on Educational Advances in Artificial Intelligence (AAAI’24/IAAI’24/EAAI’24)*. AAAI Press, Article 1402, 9 pages. doi:10.1609/aaai.v38i11.29150

- [14] Aryamaan Jain, Avinash Sharma, and Rajan. 2023. Adaptive & Multi-Resolution Procedural Infinite Terrain Generation with Diffusion Models and Perlin Noise. In *Proceedings of the Thirteenth Indian Conference on Computer Vision, Graphics and Image Processing (Gandhinagar, India) (ICVGIP '22)*. Association for Computing Machinery, New York, NY, USA, Article 55, 9 pages. doi:10.1145/3571600.3571657
- [15] Álvaro Barbero Jiménez. 2023. Mixture of Diffusers for scene composition and high resolution image generation. doi:10.48550/arXiv.2302.02412 arXiv:2302.02412 [cs].
- [16] Tero Karras, Miika Aittala, Tuomas Kynkäänniemi, Jaakko Lehtinen, Timo Aila, and Samuli Laine. 2024. Guiding a Diffusion Model with a Bad Version of Itself. In *Proc. NeurIPS*.
- [17] Tero Karras, Miika Aittala, Jaakko Lehtinen, Janne Hellsten, Timo Aila, and Samuli Laine. 2024. Analyzing and Improving the Training Dynamics of Diffusion Models. In *Proc. CVPR*.
- [18] Yuseung Lee, Kunho Kim, Hyunjin Kim, and Minhyuk Sung. 2023. SyncDiffusion: Coherent Montage via Synchronized Joint Diffusions. In *Advances in Neural Information Processing Systems*, A. Oh, T. Naumann, A. Globerson, K. Saenko, M. Hardt, and S. Levine (Eds.), Vol. 36. Curran Associates, Inc., 50648–50660. [https://proceedings.neurips.cc/paper\\_files/paper/2023/file/9ee3a664ccfeabc0da16ac6f1f1cfe59-Paper-Conference.pdf](https://proceedings.neurips.cc/paper_files/paper/2023/file/9ee3a664ccfeabc0da16ac6f1f1cfe59-Paper-Conference.pdf)
- [19] Sikuang Li, Chen Yang, Jiemin Fang, Taoran Yi, Jia Lu, Jiazhong Cen, Lingxi Xie, Wei Shen, and Qi Tian. 2025. WorldGrow: Generating Infinite 3D World. doi:10.48550/arXiv.2510.21682 arXiv:2510.21682 [cs].
- [20] Chieh Hubert Lin, Hsin-Ying Lee, Yen-Chi Cheng, Sergey Tulyakov, and Ming-Hsuan Yang. 2022. InfinityGAN: Towards Infinite-Pixel Image Synthesis. In *International Conference on Learning Representations*. <https://openreview.net/forum?id=ufGMqIM0a4b>
- [21] Cheng Lu and Yang Song. 2025. Simplifying, Stabilizing and Scaling Continuous-time Consistency Models. In *The Thirteenth International Conference on Learning Representations*. <https://openreview.net/forum?id=LyJi5ugyJx>
- [22] NOAA National Geophysical Data Center. 2009. ETOPO1 1 Arc-Minute Global Relief Model. doi:10.7289/V5C8276M
- [23] Ken Perlin. 1985. An image synthesizer. In *Proceedings of the 12th annual conference on Computer graphics and interactive techniques - SIGGRAPH '85*. ACM Press, Not Known, 287–296. doi:10.1145/325334.325247
- [24] Ken Perlin. 2002. Improving noise. In *Proceedings of the 29th annual conference on Computer graphics and interactive techniques*. ACM, San Antonio Texas, 681–682. doi:10.1145/566570.566636
- [25] Robin Rombach, Andreas Blattmann, Dominik Lorenz, Patrick Esser, and Björn Ommer. 2021. High-Resolution Image Synthesis with Latent Diffusion Models. arXiv:2112.10752 [cs.CV]
- [26] Ansh Sharma, Albert Xiao, Praneet Rathi, Rohit Kundu, Albert Zhai, Yuan Shen, and Shenlong Wang. 2024. EarthGen: Generating the World from Top-Down Views. doi:10.48550/arXiv.2409.01491 arXiv:2409.01491 [cs].
- [27] Jascha Sohl-Dickstein, Eric Weiss, Niru Maheswaranathan, and Surya Ganguli. 2015. Deep Unsupervised Learning using Nonequilibrium Thermodynamics. In *Proceedings of the 32nd International Conference on Machine Learning (Proceedings of Machine Learning Research, Vol. 37)*, Francis Bach and David Blei (Eds.). PMLR, Lille, France, 2256–2265. <https://proceedings.mlr.press/v37/sohl-dickstein15.html>
- [28] Yang Song, Prafulla Dhariwal, Mark Chen, and Ilya Sutskever. 2023. Consistency models. In *Proceedings of the 40th International Conference on Machine Learning (ICML '23)*. JMLR.org, Honolulu, Hawaii, USA.
- [29] Ryan Rs Spick and James Walker. 2019. Realistic and Textured Terrain Generation using GANs. In *European Conference on Visual Media Production*. ACM, London United Kingdom, 1–10. doi:10.1145/3359998.3369407
- [30] Georgios Voulgaris, Ioannis Mademlis, and Ioannis Pitas. 2021. Procedural Terrain Generation Using Generative Adversarial Networks. In *2021 29th European Signal Processing Conference (EUSIPCO)*. IEEE, Dublin, Ireland, 686–690. doi:10.23919/EUSIPCO54536.2021.9616151
- [31] Zhennan Wu, Yang Li, Han Yan, Taizhang Shang, Weixuan Sun, Senbo Wang, Ruikai Cui, Weizhe Liu, Hiroyuki Sato, Hongdong Li, and Pan Ji. 2024. Block-Fusion: Expandable 3D Scene Generation using Latent Tri-plane Extrapolation. *ACM Transactions on Graphics* 43, 4 (2024). doi:10.1145/3658188
- [32] Dai Yamazaki, Daiki Ikeshima, Ryunosuke Tawatari, Tomohiro Yamaguchi, Fiachra O’Loughlin, Jeffery C. Neal, Christopher C. Sampson, Shinjiro Kanae, and Paul D. Bates. 2017. A high-accuracy map of global terrain elevations. *Geophysical Research Letters* 44, 11 (June 2017), 5844–5853. doi:10.1002/2017GL072874
- [33] Xiaoyu Zhang, Teng Zhou, Xinlong Zhang, Jia Wei, and Yongchuan Tang. 2025. Multi-Scale Diffusion: Enhancing Spatial Layout in High-Resolution Panoramic Image Generation. In *2025 IEEE International Conference on Multimedia and Expo (ICME)*. IEEE Computer Society, Los Alamitos, CA, USA, 1–6. doi:10.1109/ICME59968.2025.11209478
- [34] Teng Zhou and Yongchuan Tang. 2024. TwinDiffusion: Enhancing Coherence and Efficiency in Panoramic Image Generation with Diffusion Models. arXiv:2404.19475 (2024). doi:10.48550/arXiv.2404.19475 arXiv:2404.19475 [cs].

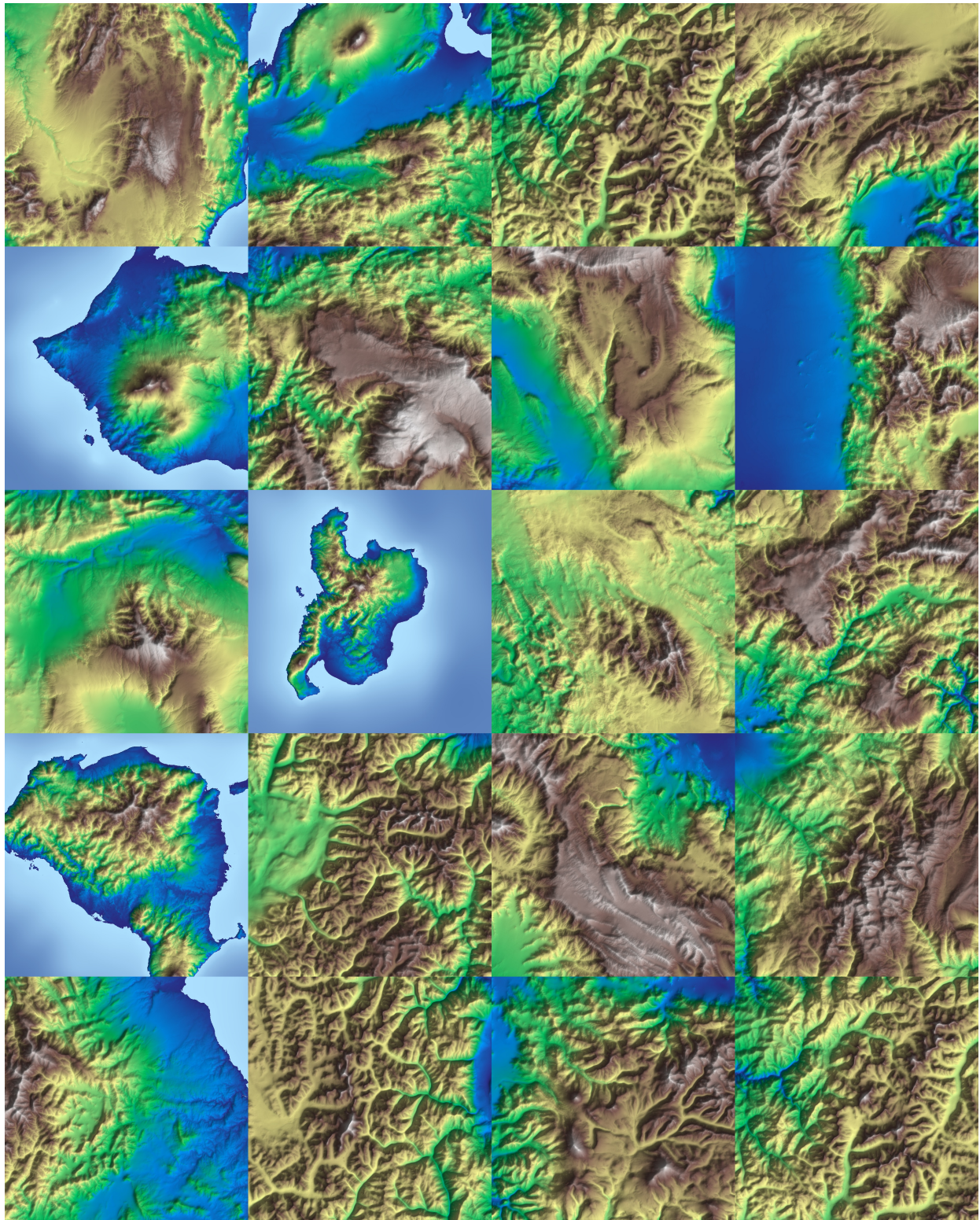


Figure 4: Twenty generated 1024 by 1024 regions from Terrain Diffusion. Samples cover volcanic islands, high relief mountain systems, and dissected plateaus, illustrating the model's ability to reproduce diverse landscapes with coherent multi-scale structure. All emerge from one world generated with the same seed as in Figure 1. Zoom for details.



Figure 5: Nine Minecraft scenes generated from Terrain Diffusion using a single fixed biome mapping derived from the model's climatic outputs. The Distant Horizons mod is used to increase render distance, and Bliss shaders are used to enhance visuals.

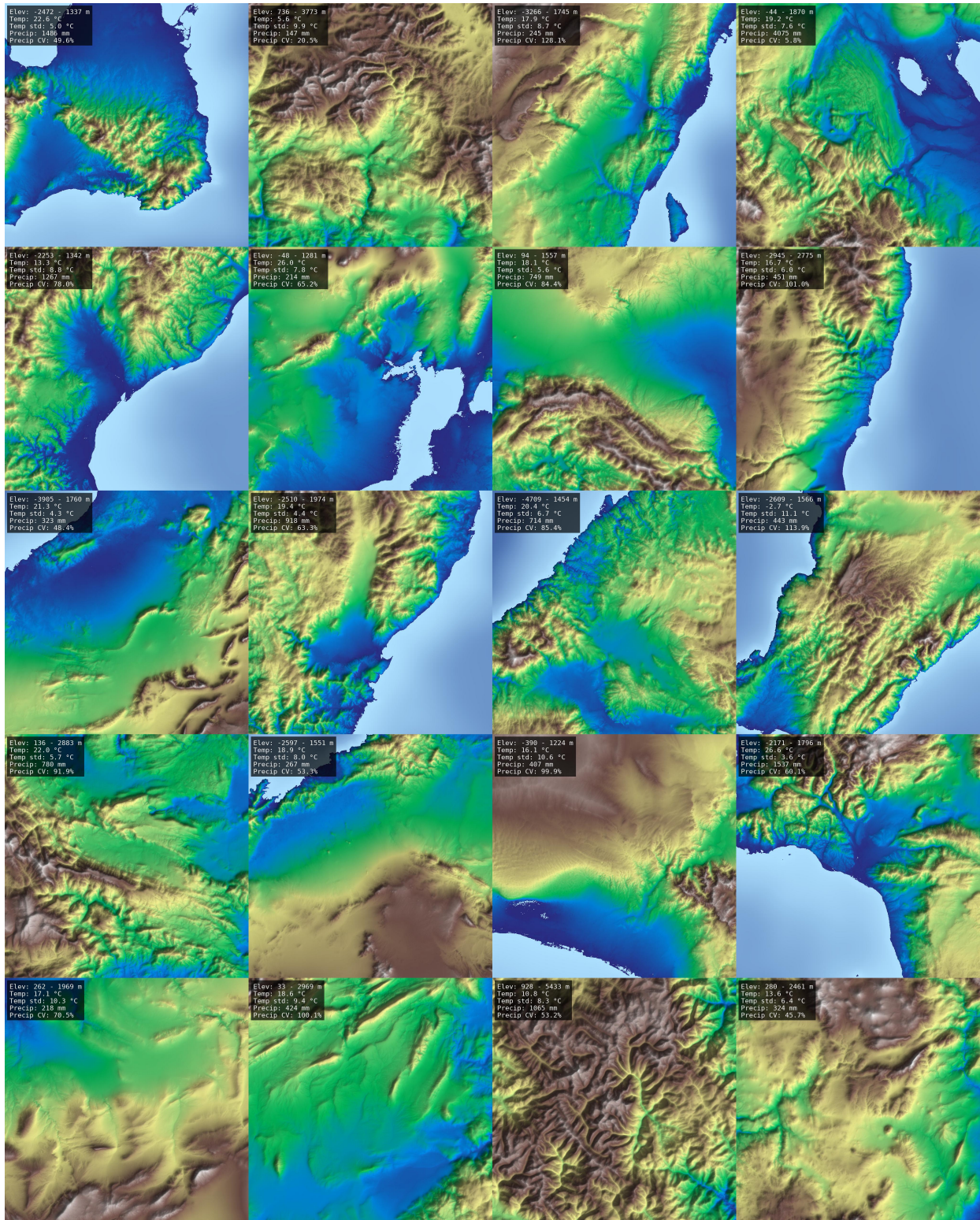


Figure 6: Twenty additional 1024 by 1024 regions from Terrain Diffusion. Samples are uncurated, except for filtering regions with more than 50% ocean. We include additional details on overall elevation range, and climate variables, in the top left of each sample.

**Table 4: Performance metrics for region generation. Megapixel throughput (MP/s) is calculated using the steady-state TTST.**

Region Size	TTFT (s) ↓	TTST (s) ↓	Peak VRAM (MB) ↓	MP/s ↑	TTFT (p5, p50, p95) ↓	TTST (p5, p50, p95) ↓
1024 × 1024	2.96s ± 0.35s	1.79s ± 0.27s	<b>2214 MB</b>	<b>0.59</b>	(2.59, 2.78, 3.74)	(1.40, 1.78, 2.30)
512 × 512	1.72s ± 0.19s	0.66s ± 0.18s	<b>2214MB</b>	0.40	(1.34, 1.76, 2.00)	(0.42, 0.62, 0.96)
256 × 256	1.25s ± 0.19s	0.26s ± 0.18s	<b>2214 MB</b>	0.25	(1.03, 1.22, 1.54)	(0.00, 0.29, 0.53)
128 × 128	<b>1.06s</b> ± 0.14s	<b>0.10s</b> ± 0.15s	<b>2214 MB</b>	0.16	(0.72, 1.09, 1.22)	(0.00, 0.00, 0.40)

## A Extended Results

### A.1 Additional Qualitative Samples

In Figure 6, we showcase twenty additional 1024 by 1024 regions from Terrain Diffusion. Samples are uncurated, except for automatically excluding regions with more than 50% ocean in the coarse map. We include additional details on overall elevation range, and climate variables, in the top left of each sample.

### A.2 Additional Details on FID Calculations

Below we provide pseudocode for the normalization scheme used to convert arbitrary elevation values to the 0-255 range required for FID calculation.

---

#### Algorithm 2 Normalizing heightmaps for FID

---

**Inputs:**

$I$  ▷ batch of single-channel images ( $B \times 1 \times H \times W$ )

$I_{\min} \leftarrow \min(I)$  ▷ Per-image minimum

$I_{\max} \leftarrow \max(I)$  ▷ Per-image maximum

$I_{\text{range}} \leftarrow \max(I_{\max} - I_{\min}, 255)$  ▷ Ensure scaling factor  $\geq 255$

$I_{\text{mid}} \leftarrow (I_{\min} + I_{\max})/2$

$I_{\text{norm}} \leftarrow \text{clamp}\left(\left(\frac{I - I_{\text{mid}}}{I_{\text{range}}} + 0.5\right) \times 255, 0, 255\right)$

$O \leftarrow \text{repeat}(I_{\text{norm}}, \text{channels} = 3)$

**Output:**  $O$  cast to uint8

---

For Perlin blending [14], our implementation differs from the reference method, which targets a zero-centered dataset. To ensure a fair comparison, we adapt the algorithm to our data: rather than applying Perlin noise with a static distribution, we employ an adaptive distribution centered on the mean and scaled by the standard deviation of surrounding elevation tiles (weighted by linear interpolation).

### A.3 Additional Performance Metrics

In addition to the latency metrics provided in the main text, we also report peak VRAM usage and additional latency metrics for varying region sizes. Our results are in Table 4. For all performance calculations, we initially compile the models with `torch.compile()`, and use full-precision inference (fp32), since it provided the best performance. VRAM usage reduces to 1846 MB with half-precision

floats. We measure latency end-to-end as observed through the same API exposed to applications, including all I/O and system overhead.

## B Formal Properties of InfiniteDiffusion

### B.1 Preliminaries and Notation

We first make precise the InfiniteDiffusion framework used in the main text.

*Infinite image space.* Let the spatial domain be the integer lattice  $\mathbb{Z}^d$ , and let

$$\mathcal{J} := \mathbb{R}^{\mathbb{Z}^d \times C}$$

denote the space of infinite images with  $C$  channels. We write  $J \in \mathcal{J}$  as a function  $J : \mathbb{Z}^d \rightarrow \mathbb{R}^C$  over pixel coordinates. For the following sections, we write  $\Omega$  as shorthand for the index-set  $[H_1] \times \dots \times [H_d]$ .

*Regions and windows.* A (rectangular) region is any subset of the form

$$R = [a_1, b_1] \times \dots \times [a_d, b_d] \subset \mathbb{Z}^d$$

with integers  $a_k < b_k$ . The set of window indices is a countable set  $S$  (e.g.  $S = \mathbb{Z}^d$ ). For each  $i \in S$  we are given a window region  $R_i \subset \mathbb{Z}^d$ , a weight map  $W_i \in \mathbb{R}^\Omega$ , and a conditioning vector  $y_i$ . We assume the window layout is such that for every finite region  $R$ , only finitely many windows intersect  $R$ :

**Assumption 1 (Finite window overlap).** For every finite region  $R$ ,

$$\kappa(R) := \{i \in S : R_i \cap R \neq \emptyset\}$$

is finite.

*Embedding operator.* For any tensor  $x \in \mathbb{R}^{\Omega \times C}$ , the operator  $U_i(x) \in \mathcal{J}$  denotes the infinite image obtained by placing  $x$  on  $R_i$  and zero elsewhere.

*Pretrained diffusion model.* Let  $\Phi$  denote a fixed pretrained denoising network acting on window-sized images. We formalize it as a deterministic function

$$\Phi : \mathbb{R}^{\Omega \times C} \times \mathcal{Y} \rightarrow \mathbb{R}^{\Omega \times C},$$

where  $\mathcal{Y}$  is the space of conditioning vectors.

*InfiniteDiffusion update.* For a given noisy image  $J_t \in \mathcal{J}$ , the InfiniteDiffusion update at step  $t \rightarrow t-1$  is defined, for any finite region  $R$ , by

$$\Psi(J_t | z)[R] = \left( \frac{\sum_{i \in \kappa(R)} U_i(W_i \otimes \Phi(J_t[R_i] | y_i))}{\sum_{j \in \kappa(R)} U_j(W_j)} \right) [R], \quad (3)$$

where  $\otimes$  denotes the Hadamard (elementwise) product and the division is also elementwise. For this update, we adopt the convention that any division by zero is defined to be zero. By Assumption 1, both sums are finite on any finite  $R$ , so (3) is well-defined.  $z$  is a (possibly infinite) vector from which the  $y_i$  are computed.

*Seeds and initial noise.* Let  $\mathcal{X}$  be a set of seeds. A seed  $s \in \mathcal{X}$  deterministically selects an initial noise field  $J_T^{(s)} \in \mathcal{J}$ , and a conditioning vector  $z^{(s)} \in \mathcal{Z}$ . Formally, there are deterministic functions

$$G : \mathcal{X} \times \mathbb{Z}^d \rightarrow \mathbb{R}^C, \quad H : \mathcal{X} \rightarrow \mathcal{Z}, \quad \Lambda : \mathcal{Z} \times S \rightarrow \mathcal{Y}$$

such that

$$J_T^{(s)}(p) = G(s, p), \quad z^{(s)} = H(s), \quad y_i^{(s)} = \Lambda(z^{(s)}, i).$$

*Definition of  $J_t^{(s)}$ .* For a fixed seed  $s$ , we define the entire trajectory  $(J_t^{(s)})_{t=0}^T$  recursively by:

- $J_T^{(s)}$  is given by  $G$ .
- For  $t = T, T-1, \dots, 1$ , define  $J_{t-1}^{(s)}$  via (3) with  $J_t = J_t^{(s)}$  and  $y_i = y_i^{(s)}$ .

Because  $T$  is finite and each update uses only finite sums on any finite region, the tensors  $J_t^{(s)}$  are well-defined for all  $t \in \{0, \dots, T\}$ .

*Lazy evaluation algorithm.* Algorithm 1 efficiently computes (3). At level  $t$  it maintains images  $A_t, B_t \in \mathcal{J}$  and a processed set  $P_t \subseteq S$ . To answer a query  $J_t[R]$ , it performs:

For each window  $i \in \kappa(R) \setminus P_t$ :

$$\begin{aligned} A_t[R_i] &\leftarrow A_t[R_i] + W_i \otimes \Phi(J_t[R_i], y_i), \\ B_t[R_i] &\leftarrow B_t[R_i] + W_i. \end{aligned}$$

Add each such  $i$  to  $P_t$ . The result is

$$J_t[R] = A_t[R] / B_t[R].$$

Where the division is performed elementwise. New windows are evaluated recursively by querying  $J_t[\cdot]$  in the same way at level  $t$ , until reaching  $J_T^{(s)}$ , which is given by the seed. At initialization,  $A_t = \mathbf{0}$ ,  $B_t = \mathbf{0}$ , and  $P_t = \emptyset$ .

We now formalize and prove the three properties stated in the main text.

## B.2 Seed Consistency

Informally, seed consistency says that once the seed is fixed, every finite region  $J_t[R]$  is a deterministic function of the seed and the region alone, and is independent of the order in which regions are queried.

*Definition B.1 (Seed-consistent generative process).* A family of random infinite images  $\{J_t\}_{t=0}^T$  on  $\mathbb{Z}^d$  is *seed-consistent* if there exists a set of seeds  $\mathcal{X}$  such that for all  $s \in \mathcal{X}$ ,  $t \in \{0, \dots, T\}$  and finite  $R$ ,

$$J_t[R]$$

is a function of  $s$  and  $R$ . Consequently, repeated queries for the same  $t, s, R$  always return the same value, irrespective of the order in which regions are requested.

We show that InfiniteDiffusion, as defined in 3, is seed-consistent.

**LEMMA B.2 (INFINITEDIFFUSION IS SEED-CONSISTENT).** *Fix a seed  $s \in \mathcal{X}$ . Then for each  $t \in \{0, \dots, T\}$  and finite region  $R$ , the tensor  $J_t^{(s)}[R]$  defined by the recursive update (3) is uniquely determined by  $s$  and  $R$ .*

**PROOF.** We proceed by backward induction on  $t$ .

*Base case ( $t = T$ ).* By construction,  $J_T^{(s)}(p) = G(s, p)$  for all  $p$ , so for any finite region  $R$ , the restriction  $J_T^{(s)}[R]$  is uniquely determined by  $s$  and  $R$ .

*Inductive step.* Assume that for some  $t \in \{1, \dots, T\}$ ,  $J_t^{(s)}[R]$  is uniquely determined by  $s$  and  $R$  for all finite regions  $R$ . Consider  $J_{t-1}^{(s)}[R]$  for a finite region  $R$ .

By definition (3),

$$J_{t-1}^{(s)}[R] = \left( \frac{\sum_{i \in \kappa(R)} U_i(W_i \otimes \Phi(J_t^{(s)}[R_i] | y_i^{(s)}))}{\sum_{j \in \kappa(R)} U_j(W_j)} \right) [R]$$

For each  $i \in \kappa(R)$ , the region  $R_i$  is finite, so by the inductive hypothesis  $J_t^{(s)}[R_i]$  is uniquely determined by  $s$  and  $R_i$ . The model  $\Phi$  and weight maps  $W_i$  are deterministic. Therefore each term

$$U_i(W_i \otimes \Phi(J_t^{(s)}[R_i] | y_i^{(s)}))$$

is uniquely determined by  $s$ , and hence the finite sums in the numerator and denominator are uniquely determined. Thus  $J_{t-1}^{(s)}[R]$  is uniquely determined by  $s$  and  $R$ .

By induction, the claim holds for all  $t$ .  $\square$

Lemma B.2 shows that InfiniteDiffusion has a well-defined deterministic output for a fixed seed. We now show that the lazy query algorithm is consistent with this definition, and is therefore also seed-consistent.

LEMMA B.3 (ALGORITHM CONSISTENCY). Fix  $s \in \mathcal{X}$  and a timestep  $t \in \{1, \dots, T\}$ . Then immediately before any query  $J_t[R]$  with Algorithm 1, the pair  $(A_t, B_t)$  satisfy

$$A_t = \sum_{i \in P_t} U_i(W_i \otimes \Phi(J_t^{(s)}[R_i] | y_i^{(s)})),$$

$$B_t = \sum_{i \in P_t} U_i(W_i).$$

Furthermore, after performing one iteration of Algorithm 1, the updated state satisfies the same form with  $P_t$  replaced by  $P_t \cup \kappa(R)$ .

PROOF. We prove this by induction over an arbitrary sequence of queries. At initialization,  $A_t = 0$ ,  $B_t = 0$ , and  $P_t = \emptyset$ , so the claim is trivially true.

Now assume that before any query  $J_{t-1}[R]$  we have

$$A_t = \sum_{i \in P_t} U_i(V_i), \quad B_t = \sum_{i \in P_t} U_i(W_i),$$

where we write  $V_i$  as shorthand for  $W_i \otimes \Phi(J_t^{(s)}[R_i] | y_i^{(s)})$ .

During the query, for each  $i \in \kappa(R) \setminus P_t$  the algorithm performs

$$A_t[R_i] \leftarrow A_t[R_i] + V_i, \quad B_t[R_i] \leftarrow B_t[R_i] + W_i$$

and does not modify any pixels outside  $R_i$ . Equivalently, this is

$$A_t \leftarrow A_t + U_i(V_i), \quad B_t \leftarrow B_t + U_i(W_i).$$

After processing all such windows we obtain

$$A_t = \sum_{i \in P_t} U_i(V_i) + \sum_{i \in \kappa(R) \setminus P_t} U_i(V_i) = \sum_{i \in P_t \cup \kappa(R)} U_i(V_i),$$

and similarly

$$B_t = \sum_{i \in P_t \cup \kappa(R)} U_i(W_i).$$

Finally, the algorithm updates  $P_t \leftarrow P_t \cup \kappa(R)$ , so the updated state satisfies the same form with  $P_t$  replaced by  $P_t \cup \kappa(R)$ .

By induction, the claim holds for all queries  $J_t[R]$ .  $\square$

We now show that Algorithm 1 is consistent with the formal definition in 3.

LEMMA B.4 (CORRECTNESS OF A SINGLE QUERY). Fix  $s, t$ , and a finite region  $R$ . After any query  $J_{t-1}[R]$  following Algorithm 1, we have

$$J_t[R] = A_t[R]/B_t[R] = J_t^{(s)}[R].$$

PROOF. By Lemma B.3, after the query finishes we have

$$A_t = \sum_{i \in P'_t} U_i(V_i), \quad B_t = \sum_{i \in P'_t} U_i(W_i),$$

for some processed set  $P'_t \supseteq \kappa(R)$ .

Now restrict to the region  $R$ . Any window  $i \notin \kappa(R)$  has  $R_i \cap R = \emptyset$ , so

$$U_i(V_i)[R] = 0, \quad U_i(W_i)[R] = 0.$$

Therefore,

$$A_t[R] = \left( \sum_{i \in P'_t} U_i(V_i) \right) [R] = \left( \sum_{i \in \kappa(R)} U_i(V_i) \right) [R],$$

and similarly

$$B_t[R] = \left( \sum_{i \in \kappa(R)} U_i(W_i) \right) [R].$$

Comparing with the definition (3), we see that

$$\frac{A_t[R]}{B_t[R]} = \Psi(J_t^{(s)} | z^{(s)})[R] = J_t^{(s)}[R],$$

which is the claim.  $\square$

We can now state the main seed consistency result.

THEOREM B.5 (SEED CONSISTENCY OF THE ALGORITHM). Under Assumption 1, the InfiniteDiffusion lazy query algorithm is seed-consistent.

PROOF. By Lemma B.2, for each  $s, t$ , and finite  $R$ ,  $J_t^{(s)}[R]$  is uniquely determined by  $(s, R)$ , so the process defined by (3) is seed-consistent. By Lemma B.4, the algorithm is equivalent, and therefore also seed-consistent.  $\square$

Theorem B.5 formalizes the informal argument in the main text: once a seed is fixed, the entire trajectory  $(J_t^{(s)})_{t=0}^T$  is fully determined, and the lazy querying and caching scheme merely memoizes a deterministic computation without affecting its outcome. In particular, querying regions in different orders or repeating a query for the same region cannot change the result.

### B.3 Constant-Time Random Access

We now formalize the claim that accessing the value on any window-sized region has constant computational cost, independent of the absolute location in the infinite domain. We measure cost in terms of the number of evaluations of  $\Phi$ , which dominate runtime in practice. Let  $C_t(R)$  denote the worst-case number of  $\Phi$ -calls required by the lazy algorithm to answer a query for  $J_t[R]$ , starting from an empty cache at all timesteps.

**Assumption 2 (Uniform overlap bound).** There exists a finite constant  $M$  such that  $|\kappa(R_i)| \leq M$  for every window region  $R_i$ . In words, each window region overlaps the regions of at most  $M$  windows.

We treat the total number of diffusion steps  $T$  and the window shape as fixed hyperparameters of the model.

LEMMA B.6 (RECURSIVE COST BOUND). *Under Assumption 2, for any timestep  $t$  and any window index  $i \in S$ , the cost  $C_t(R_i)$  satisfies*

$$C_t(R_i) \leq M(1 + \sup_{j \in S} C_{t+1}(R_j)) \quad \text{for } t < T,$$

with base case  $C_T(R_i) = 0$  for all  $i$ .

PROOF. Consider a query for  $J_t[R_i]$  at some  $t < T$ . By the update rule, computing this query requires evaluating  $\Phi(J_{t+1}[R_k], y_k)$  for every  $k \in \kappa(R_i)$ .

Each such evaluation requires one call to  $\Phi$  at level  $t$ , and in order to provide the input  $J_{t+1}[R_k]$ , the algorithm may in turn need to perform some number of step- $(t+1)$  queries. That is, for each  $k \in \kappa(R_i)$  we incur cost  $1 + C_{t+1}(R_k)$ .

The cardinality of  $\kappa(R_i)$  is at most  $M$  by Assumption 2. Thus

$$C_t(R_i) \leq \sum_{k \in \kappa(R_i)} (1 + C_{t+1}(R_k)) \leq M(1 + \sup_{j \in S} C_{t+1}(R_j))$$

At the top level  $t = T$ , no further calls to  $\Phi$  are required because  $J_T$  is given directly by the noise generator, hence  $C_T(R_i) = 0$ .  $\square$

THEOREM B.7 (UNIFORM BOUND ON COST FOR WINDOW REGIONS). *Under Assumption 2, there exists a constant  $K$  depending only on  $T$  and  $M$  such that for all  $t$  and all window indices  $i$ ,*

$$C_t(R_i) \leq K.$$

PROOF. Let

$$c_t := \sup_{i \in S} C_t(R_i).$$

By Lemma B.6,

$$c_t \leq M(1 + c_{t+1}), \quad t < T,$$

with  $c_T = 0$ .

Unwinding this recurrence yields

$$c_{T-1} \leq M(1 + 0) = M, \quad c_{T-2} \leq M(1 + c_{T-1}) \leq M + Mc_{T-1},$$

and in general

$$c_t \leq M + M^2 + \dots + M^{T-t}.$$

For fixed  $T$  and  $M$ , the right-hand side is a finite constant independent of  $i$  and the absolute location of  $R_i$  in the plane. Taking

$$K := M + M^2 + \dots + M^T$$

gives the claimed uniform bound.  $\square$

For any window index  $i$ , Theorem B.7 gives a uniform bound  $C_0(R_i) \leq K$  on the number of calls to  $\Phi$  needed to answer a query for  $J_0[R_i]$ , starting from an empty cache. This bound depends only on  $T$  and  $M$ , which are constants, and not on  $i$  or any regions previously processed. In standard algorithmic notation, this means that the time complexity of a query  $J_0[R]$  is  $O(1)$ , when  $R$  is a window

region. Queries typically cost far less than  $K$ , but this is not required for the asymptotic guarantee.

Combined with seed consistency, Theorem B.7 formally justifies the claim that users can jump to arbitrary locations in the infinite world and query any window region efficiently, without needing to generate intermediate tiles and without affecting the content of the regions. When we assume that any region of fixed size has a bounded number of window overlaps, the same argument applies to arbitrary regions of bounded size, not just individual windows.

## B.4 Parallelization

Finally, we formalize the statement that InfiniteDiffusion admits parallel evaluation of window updates at any fixed timestep.

Recall that, at fixed  $t$  and seed  $s$ , the numerator and denominator images for the update  $J_{t+1}^{(s)} \mapsto J_t^{(s)}$  are

$$A_t^{(s)} = \sum_{i \in S} U_i(W_i \otimes \Phi(J_{t+1}^{(s)}[R_i] \mid y_i^{(s)})),$$

$$B_t^{(s)} = \sum_{i \in S} U_i(W_i),$$

The updated image is then

$$J_t^{(s)} = A_t^{(s)} / B_t^{(s)}.$$

We treat calls to  $\Phi$  as the only expensive operation, and all other operations (additions, multiplications, divisions and updates to  $A_t, B_t$ ) as free. In this work, a computation is *parallelizable* if there exists an algorithm in which all calls to  $\Phi$  can be partitioned into a constant number of *rounds* so that within each round the calls are independent and can be executed simultaneously.

We first note that, at a fixed timestep, once the inputs  $J_{t+1}^{(s)}[R_i]$  are known, all required model evaluations can be done in parallel.

LEMMA B.8 (PARALLEL WINDOW UPDATES AT A FIXED TIMESTEP). *Fix a seed  $s$ , a timestep  $t \in \{0, \dots, T-1\}$ , and a finite set of window indices  $I \subseteq S$ . Suppose that for every  $i \in I$  the tensor  $J_{t+1}^{(s)}[R_i]$  is available for free. Then the evaluations*

$$\Phi(J_{t+1}^{(s)}[R_i] \mid y_i^{(s)}), \quad i \in I,$$

*can be performed in a single parallel round, and all corresponding contributions to  $A_t^{(s)}$  and  $B_t^{(s)}$  on  $\bigcup_{i \in I} R_i$  can be formed without any further calls to  $\Phi$ .*

PROOF. For each  $i \in I$ , the input to  $\Phi$  depends only on  $J_{t+1}^{(s)}[R_i]$  and  $y_i^{(s)}$ , which are both already available. Thus the evaluations  $\Phi(J_{t+1}^{(s)}[R_i] \mid y_i^{(s)})$  are mutually independent and can be carried out simultaneously.

Once these outputs are known, the updates

$$A_t^{(s)} \leftarrow A_t^{(s)} + U_i(W_i \otimes \Phi(J_{t+1}^{(s)}[R_i] \mid y_i^{(s)}))$$

$$B_t^{(s)} \leftarrow B_t^{(s)} + U_i(W_i)$$

and the division  $J_t^{(s)} = A_t^{(s)} / B_t^{(s)}$  involve only element-wise arithmetic and therefore require no additional model evaluations. Hence all work associated with the windows in  $I$  can be completed using a single parallel round of calls to  $\Phi$ .  $\square$

We now show that answering any finite collection of region queries at any timestep admits a parallel schedule of model evaluations.

**THEOREM B.9 (PARALLELIZATION OF FINITE QUERY SETS).** *Fix a seed  $s$ , a timestep  $t \in \{0, \dots, T\}$ , and a finite collection of regions*

$$\mathcal{R} = \{R^{(1)}, \dots, R^{(m)}\}.$$

*Consider the computation that evaluates  $J_t^{(s)}[R^{(k)}]$  for all  $k = 1, \dots, m$  using the recursive update (3), starting from  $J_T^{(s)}$  and without caching. Then all calls to  $\Phi$  required by this computation can be arranged into at most  $T - t$  parallel rounds.*

**PROOF.** By Lemma B.2, once  $s$  is fixed the values  $J_u^{(s)}[R]$  are uniquely determined for all  $u$  and all finite regions  $R$ . In particular, the set of model evaluations that appear in the recursive computation of  $\{J_t^{(s)}[R^{(k)}]\}_{k=1}^m$  is fixed; only their order of execution is not.

We prove the claim by backward induction on  $t$ .

*Base case ( $t = T$ ).* By definition,  $J_T^{(s)}$  is given directly by the noise generator  $G$  and does not require any calls to  $\Phi$ . Thus any finite set of queries at  $t = T$  is trivially parallelizable with zero rounds.

*Inductive step.* Fix  $t < T$  and assume the statement holds for  $t + 1$ . Consider a finite collection  $\mathcal{R} = \{R^{(1)}, \dots, R^{(m)}\}$  of regions at time  $t$ .

Let

$$R^* := \bigcup_{k=1}^m R^{(k)}$$

be the union of all queried regions at level  $t$ . By Assumption 1, only finitely many windows intersect  $R^*$ , so the index set

$$I_t := \kappa(R^*) = \{i \in S : R_i \cap R^* \neq \emptyset\}$$

is finite. By (3), computing  $J_t^{(s)}[R^{(k)}]$  for all  $k$  requires knowing the regions  $J_{t+1}^{(s)}[R_i]$  for all  $i \in I_t$ .

Each region  $R_i$  is finite, and from the recursion defining  $J_t^{(s)}$  we see that  $J_t^{(s)}[R_i]$  itself is obtained from regions of the form  $J_{t+1}^{(s)}[R_j]$  for windows  $j$  that intersect  $R_i$ . Let  $\mathcal{R}_{t+1}$  denote the (finite) collection of all such window regions  $R_j$  at timestep  $t + 1$  that are needed in this way. By the induction hypothesis applied at level  $t + 1$  to the finite set  $\mathcal{R}_{t+1}$ , all model evaluations needed to compute  $\{J_{t+1}^{(s)}[R_j] : R_j \in \mathcal{R}_{t+1}\}$  can be scheduled in at most  $T - (t + 1)$  parallel rounds.

Once all these regions are available, the corresponding values  $J_t^{(s)}[R_i]$  for  $i \in I_t$  are determined and can be formed without further calls to  $\Phi$ . At this point, Lemma B.8 implies that all remaining

evaluations

$$\Phi(J_{t+1}^{(s)}[R_i] \mid y_i^{(s)}), \quad i \in I_t,$$

required to construct  $A_t^{(s)}$  and  $B_t^{(s)}$  on  $R^*$  can be carried out in a single additional parallel round. No more model evaluations are needed to extract  $J_t^{(s)}[R^{(k)}]$  from these images.

Thus, the entire computation for the queries  $\mathcal{R}$  at timestep  $t$  can be performed using at most

$$1 + (T - (t + 1)) = T - t$$

parallel rounds of calls to  $\Phi$ . This completes the induction.  $\square$

Theorem B.9 shows that for any fixed seed  $s$ , timestep  $t$  and finite collection of regions  $\mathcal{R}$ , the recursive computation of  $\{J_t^{(s)}[R] : R \in \mathcal{R}\}$  admits a bounded-depth parallel schedule of diffusion model evaluations. Combined with seed consistency, this formalizes the claim in the main text that all diffusion model evaluations required to serve any finite batch of queries  $J_t^{(s)}[R]$  can be performed in parallel, up to the intrinsic sequential dependence across diffusion steps.

## C The Infinite Tensor Framework

To support the computational requirements of InfiniteDiffusion, specifically the need for bounded-memory operations on unbounded domains, we developed infinite-tensor. This open-source Python library<sup>3</sup> abstracts the management of sliding windows, caching, and dependency chaining, allowing the implementation of diffusion models to remain focused on mathematical operations rather than memory management.

### C.1 Core Abstractions

The framework treats an infinite tensor  $\mathcal{T}$  not as a stored array of data, but as a lazily evaluated, immutable object defined by a deterministic generator function  $f$ . For context, we typically store the accumulators  $A_t$  and  $B_t$  from Section 3.3 as one infinite tensor with an extra channel for the weights  $B_t$ .

- **Infinite Tensors:** A tensor is defined by a shape  $(S_1, \dots, S_d)$ , where any dimension  $S_i$  may be infinite (represented as None). The tensor is backed by a generator function  $f$  rather than raw memory.
- **Windows:**  $f$  operates on fixed-size *windows*. A window is defined by its size  $(H, W)$ , stride  $s \in \mathbb{Z}^2$  and offset  $o \in \mathbb{Z}^2$ .
- **The TileStore:** All tensors are managed by a `TileStore`, which acts as the central registry for memory management and caching. It ensures that repeated access to the same spatial region retrieves cached data rather than re-triggering computation, and ensures that dependencies between tensors are tracked. `TileStore`'s may be linked to a file for persistent storage.

<sup>3</sup>Available at <https://github.com/xandergos/infinite-tensor>

## C.2 Caching Strategies

The framework currently implements two caching mechanisms for storing an infinite tensor  $\mathcal{T}$ . These are configured via the `cache_method` parameter during tensor creation.

*Direct Caching* (`cache_method='direct'`). This method uses direct memoization of the function  $f$ . When a window is computed, its output is stored in an LRU (Least Recently Used) cache. Essentially, we store the  $x$  in  $\mathcal{T}[R_i] \leftarrow \mathcal{T}[R_i] + x$  and reconstruct  $\mathcal{T}[R]$  on demand (assuming  $\mathcal{T} = \mathbf{0}$  initially) by revisiting all the window regions  $R_i$  intersecting  $R$ . The primary benefit of this method is that users can specify a strict memory limit (e.g., `cache_limit=10MB`), which is managed through an LRU cache or a similar method. Direct caching is ideal for transient inference where minimal RAM usage is a priority, and persistent storage is undesirable.

*Indirect Caching* (`cache_method='indirect'`). This method implements the accumulation buffer strategy directly. The outputs of overlapping windows are accumulated into fixed-size storage tiles. Overall disk/memory usage is lower since overlapping regions use shared storage. However, fine-grained eviction is difficult, so disk use is unbounded. Storage is, however, highly efficient, making this method ideal for workflows utilizing persistent storage.

## C.3 Dependency Chaining and DAGs

The framework supports the construction of directed acyclic graphs (DAGs) of infinite tensors. A tensor  $\mathcal{T}_{child}$  can declare a dependency on  $\mathcal{T}_{parent}$ . When a region of  $\mathcal{T}_{child}$  is requested: 1. The framework calculates the required covering region of  $\mathcal{T}_{parent}$ . 2. The parent region is fetched (triggering upstream generation if necessary). 3. The parent data is sliced and passed to the child’s generator function  $f$ .

This allows for the construction of complex hierarchical pipelines (e.g., Coarse Model  $\rightarrow$  Latent Model  $\rightarrow$  Decoder) where each stage is an infinite tensor depending on the previous one.

## D Additional Implementation Details

An overview of our architecture with hyperparameters is provided in Table 5.

The generative components of Terrain Diffusion are built upon the EDM2 architecture [17]. We modify the base architecture, following sCM [21], by implementing pixel-norm on embedding vectors and substituting Fourier embeddings with Positional embeddings. To incorporate auxiliary conditioning, we utilize a magnitude-preserving linear layer to project flattened conditioning inputs

*Fidelity Optimization.* For both the core latent and decoder models, we optimize fidelity using AutoGuidance [16]. Hyperparameter sweeps are conducted via Optuna, minimizing Kernel Inception Distance (KID) [4] calculated over 1,000 samples. We terminate the sweeps after 300 runs, or once KID improvement saturates.

*Consistency Distillation.* The core latent model and decoder are distilled into continuous-time consistency models (sCM). We perform post-hoc sweeps for the EMA parameter ( $\sigma_{rel}$ ) and the optimal stopping iteration. This prevents fidelity degradation observed during late-stage training.

*Training Speed.* The entire pipeline can be trained from scratch on a top-tier consumer-grade GPU (e.g., RTX 5090) in approximately one week, enabling practical retraining on custom datasets. If the decoder is reused, fine tuning the base model can be completed in about a day.

## E Dataset Details

Our dataset combines multiple global sources to provide consistent coverage of both land and ocean. Land elevations are drawn from the 3-arc-second MERIT DEM [32], while ocean bathymetry is taken from the 30-arc-second ETOPO dataset [22]. Since ETOPO’s resolution is lower, it is blurred and upsampled to match MERIT’s resolution before merging. To ensure smooth coastal transitions, we measure the distance of each ocean pixel from the nearest coastline and linearly interpolate elevation from 0 m at the shore to the local ocean depth 100 pixels offshore. To support climatic conditioning, we supplement elevation with 30-arc-second WorldClim [7] data for temperature and precipitation.

For efficient processing, data is downloaded and stored in contiguous  $2048 \times 2048$  tiles, each covering equal surface area at approximately 90m resolution. To maintain uniform ground resolution, tiles are stretched in longitude so that each pixel represents roughly the same area regardless of latitude. This equal-area tiling ensures consistent scale across training and allows all models to train on data without distortion. We also exclude tiles beyond 60 (absolute) degrees of latitude to focus on higher quality data at mid latitudes. Finally, 80% of the tiles are randomly assigned to the train set, and the remainder are withheld for validation.

All models are trained on random crops drawn from random tiles, with sampling biased so that 99% of tiles contain at least 1% land, as ocean regions are simpler and lower priority. Each crop is randomly flipped and rotated in 90 degree increments to reflect our goal of generating infinite, directionless terrain. We include scripts for reproducing the dataset in our open-source repository: <https://github.com/xandergos/terrain-diffusion>.

## F Signed Square-Root Transform

The signed square-root transform applies the function

$$f(x) = \text{sign}(x)\sqrt{|x|}$$

to each pixel of the dataset. After inference, we undo this operation with

$$f^{-1}(x) = \text{sign}(x)x^2.$$

The statistical effects of this transform are visualized in Figure 7.

Table 5: Hyperparameters and architectural details for the component models.

Parameter	Core Latent	Consistency Decoder	Coarse Model	Autoencoder
Base Architecture	EDM2 + sCM	EDM2 + sCM	EDM2 + sCM	EDM2 + sCM - Skips
Model Channels	192 (128 Guide)	64 (32 Guide)	128	64
Channel Multipliers	[1, 2, 3, 4]	[1, 2, 3, 4]	[1, 2, 3, 4]	[1, 2, 4, 4]
Layers per Block	3	3	2	2
Training Crop Size	64 × 64 (Latent)	128 × 128	16 × 16	128 × 128
Dropout	10%	0%	10%	0%
LR (Training)	$5 \times 10^{-3}$ ( $1 \times 10^{-2}$ Guide)	$1 \times 10^{-2}$	$1 \times 10^{-2}$	$1 \times 10^{-2}$
LR (Distillation)	$5 \times 10^{-5}$	$1 \times 10^{-4}$	–	–
Batch Size	48 (64 Guide)	64	256	64
Training Steps	1,024,000	716,800	153,600	153,600
Guide Training Steps	102,400	102,400	–	–
Distillation Steps	25,600	25,600	–	–
Guidance	AutoGuidance	AutoGuidance	–	–
<i>Guidance Hyperparameters</i>				
Main EMA $\sigma_{rel}$	0.12	0.093	–	–
Guide EMA $\sigma_{rel}$	0.14	0.243	–	–
Guide Stopping Step	57,344	70,656	–	–
Guidance Scale	2.15	1.26	–	–
<i>Consistency / Distillation Hyperparameters</i>				
Intermediate Timestep ( $\sigma$ )	0.35	One-Step or 0.065	–	–
$\sigma_{rel}$	0.08	0.21	–	–
EMA Step	69,632	60,416	–	–

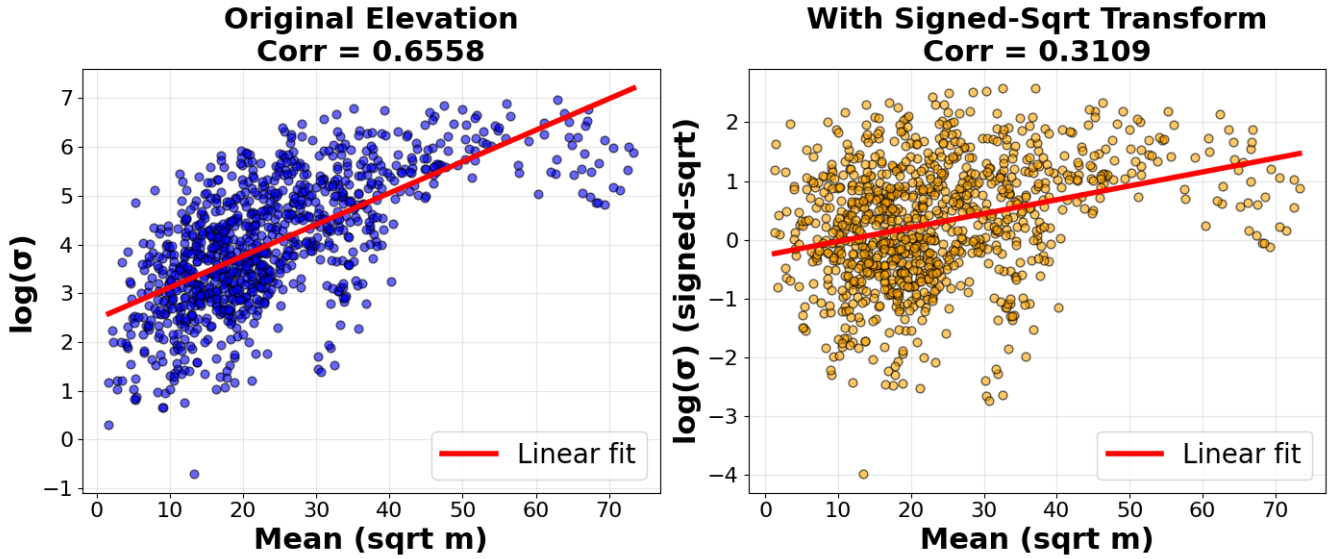


Figure 7: Effects of the signed-sqrt transform. Standard deviation become more uniformly distributed with respect to mean elevation, and the range of standard deviations compress.